J. Membrane Biol. 109, 53–64 (1989)

The Journal of
Membrane Biology

Amine Spin Probe Permeability in Sonicated Liposomes

A. Paul Todd*, Rolf J. Mehlhorn, and Robert I. Macey
Department of Physiology-Anatomy, University of California, Berkeley, California 94720

Summary. Permeabilities for an homologous series of amine nitroxide spin probes were measured in liposomes of varying composition by an electron paramagnetic resonance (EPR) method. Results show that the rate-limiting step in permeation is not adsorption/desorption at the aqueous/membrane interface for two probes in phosphatidylcholine/phosphatidic acid liposomes and for one probe in phosphatidylcholine/cholesterol/phosphatidic acid liposomes. Accordingly, we interpret observed selectivity patterns for the entire series of probes in liposomes and red cells in terms of the properties of the bilayer interior.

Results are inconsistent with simple applications of either free volume or hydrocarbon sheet models of nonelectrolyte permeation. In the former case, it was found that liposomes do not select against these probes on the basis of molecular volume. In the latter case, probe permeabilities are all much lower than would be predicted for a sheet of bulk hydrocarbon and the polarity of the rate-limiting region is shown to be greater than bulk hydrocarbon. Together with the results of previous studies of spin-labeled solutes in membranes, as well as studies of lipid dynamics in membranes, these latter results suggest that the rate-limiting region in nonelectrolyte permeation is not in the center of the bilayer, but in the relatively ordered acyl chain segments near the glycerol backbone.

Key Words EPR spin probe · liposome · membrane permeability · nonelectrolyte · order parameter · partition coefficient

Introduction

This is the second in a series of two papers on the membrane permeability of an homologous series of nonelectrolyte spin probes. In the first paper (Todd, Mehlhorn & Macey, 1989), we described a stopped-flow EPR method for measuring permeability coefficients of spin probes in suspensions of cells or vesicles and reported values for human red blood cells. In this paper, we extend these measurements to sonicated liposomes of varying composition.

Liposomes are a useful model membrane system for biophysical studies in part because, unlike planar bilayers, their composition is precisely controllable as are the contents of the internal and external compartments. However, their use in the investigation of nonelectrolyte permeability has been limited because of the difficulty of obtaining vesicles large enough to permit time resolution of permeant kinetics, while uniform enough to permit calculation of permeability coefficients. Two groups have followed the same strategy of observing the osmotic shrinking and swelling of multilamellar liposomes by light scattering in response to an osmotic gradient of the permeant molecule (deGier, Mandersloot & van Deenen, 1968; Cohen & Bangham, 1972; Cohen, 1975*a*,*b*). Multilamellar liposomes, by virtue of their large size and multiple bilayers, provide a solution to the time resolution problem for many solutes, but sacrifice uniformity. Consequently, it was possible to report only relative rates for different solutes in such studies.

In contrast, sonicated liposomes are predominantly unilamellar, of nearly uniform size, and are easier to prepare than large unilamellar vesicles of similar size uniformity. However, their small volume/area ratio is a mixed blessing. It is a limitation because the uptake of most nonelectrolytes is too fast to be resolved. In this paper, we circumvent this problem by using titratable probes far from their pK_a. On the other hand, a small volume/area ratio implies a high concentration of lipid per unit internal volume. This allows us to monitor binding of spin probe to the membrane and its redistribution across the membrane from changes in EPR signal amplitude (*cf.* Cafiso & Hubbell, 1982). Thus, we are able to distinguish the kinetics of the initial binding step from intramembrane diffusion in permeation.

Materials and Methods

Spin probes, EPR instrumentation, internal volume measurements, rapid-mix experiments and curve fitting were as described in Todd et al. (1989).

* *Present address:* Jules Stein Eye Institute, University of California, Los Angeles, CA 90024.

Lipids

Crude egg phosphatidylcholine (type IX-E) was obtained from Sigma and purified according to the method of Singleton et al. (1965). Purified lipid in 9 : 1 chloroform : methanol was dried in a rotary evaporator, weighed and redissolved in chloroform. The concentration of phospholipid was determined from total inorganic phosphate by a modification of the method of Bartlett (Kates, 1972). Purity was checked by thin-layer chromatography using silica gel plates (type IB2-F, J. T. Baker Chemical) and chloroform : methanol : water (65 : 25 : 4) as developing solvent. Lipid was visualized by incubating developed plates in iodine vapor. Ten μg of purified phosphatidylcholine (PC) was observed to migrate as a single spot.

Egg phosphatidic acid (PA) and egg sphingomyelin (SM) were obtained from Avanti Polar Lipids. Cholesterol (CL) was obtained from Calbiochem (C grade), recrystallized in ethanol and redissolved in chloroform. All lipids were stored at −17°C.

Solutions

Citrate buffer was prepared by titrating 100 mM sodium citrate with 300 mM citric acid to pH 4. The osmolarity was checked with a Wescor 5500 vapor pressure osmometer and the appropriate dilution made with distilled water to obtain a final osmolarity of~290 mmol/kg. Paramagnetic quenching buffer was prepared by titrating 100 mM $Na_2MnEDTA$ or 100 mM (tetramethylammonium)$_2$MnEDTA with 300 mM citric acid to pH 4 and the osmolarity adjusted as above.

Preparation of Liposomes

Lipid in chloroform was dried in 15-ml Corex centrifuge tubes under a stream of nitrogen, then under vacuum for ≃12 hr. After addition of buffer, sonication was performed with a Branson sonifier (model 350) at lowest power with tapered microtip. During sonication, the sample tube was cooled by immersion in a beaker of water and kept under a nitrogen atmosphere to inhibit lipid oxidation. Sonication times varied depending on lipid composition and pH. The endpoint was recognized by a characteristic translucent appearance of the suspension. Following sonication, the liposome suspension was centrifuged at 27,000 × g for 10 min to pellet metal from the sonicator tip and any undispersed lipid. The final concentration of total lipid was determined by dry weight. Drying was accomplished under vacuum until a constant weight was obtained.

Liposome Size, Volume/Area Ratio

The average radius and volume/area ratio for a suspension of nearly uniformly sized liposomes was estimated from measurements of the internal volume of the suspension, the concentration of lipid, the bilayer thickness, and the surface area per lipid molecule (*cf.* Huang & Mason, 1978). Internal volumes were measured as in the previous paper. Bilayer thicknesses and lipid surface areas are taken from hydrodynamic or x-ray diffraction studies (*see* Table 1). If $N_j \equiv$ number of molecules/cm^3 for lipid "j", $A_j \equiv$ surface area per "j" lipid molecule, and $A_t \equiv$ total surface area/cm^3, then

$$A_t = \Sigma N_j A_j. \tag{1}$$

Let $V \equiv$ internal aqueous volume/cm^3, $r_{in} \equiv$ liposome internal radius, and $\Delta r \equiv$ bilayer thickness. We can then make the following equality:

$$\frac{A_t}{V} = \frac{3(r_{in}^2 + [r_{in} + \Delta r]^2)}{r_{in}^3}. \tag{2}$$

With an assumed bilayer thickness, Δr, this cubic equation can be solved for r_{in} using the Newton-Raphson algorithm (Lanczos, 1956). We take as the effective radius the average of the inner and outer radii. The volume/area ratio pertinent to permeability calculations is then $(r_{in} + \Delta r/2)/3$.

Results

Average Liposome Sizes, Distributions

Average liposome diameters were calculated as described in Materials and Methods, assuming hydrodynamically derived values for lipid surface areas and bilayer thicknesses. They are in substantial agreement with diameters obtained directly from hydrodynamic measurements for similar liposome preparations (Johnson, 1973), as can be seen in Table 1. Negative stain and platinum shadowing electron microscopy indicate somewhat larger average diameters (270–285 *A*) for PC/PA (96 : 4) liposomes (Castle & Hubbell, 1976). We use the hydrodynamically derived radii and bilayer thicknesses in computing the volume/area ratios for permeability measurements because of their consistency with our own internal volume measurements.

It is important to consider the consequences of liposome size heterogeneity on permeability determinations. We provide a brief mathematical discussion of this problem in the Appendix. Experimentally, Castle and Hubbell (1976) found that sonicated PC/PA liposomes followed a somewhat skewed Gaussian distribution, as determined by platinum shadowing and negative stain electron microscopy. For PC/PA (96 : 4) sonicated liposomes, they obtained a standard deviation that was ≃33% of the mean by both techniques. Assuming that their distribution does not depart too drastically from a true Gaussian, we can use Table A.1 (Appendix) to estimate the probable error in calculated permeability coefficients from assuming a uniform liposome population.

If the total internal volume fraction of the suspension were 10% (unrealistically large for a suspension of sonicated liposomes) and given a 33% SD, we interpolate an error of about −18%. That is, we would calculate a permeability that is too low by 18%. This magnitude of error is not important for our purposes and will be the same for all solutes.

Table 1. Average dimensions for sonicated liposomes

	Measured diameter (*A*)	Δr	*V*/*A*	Calculated diameter
PC	204 ± 8[a]	37 ± 2	40.2 ± 2.7	235
PC/PA (96 : 4)	234 ± 9[a]	39 ± 2	45.5 ± 3.0	270
PC/CL/PA (70 : 26 : 4)	262 ± 10[a]	34 ± 2	49.3 ± 3.3	280
PC/CL/PA (48 : 50 : 2)	362 ± 14[a]	45 ± 3	113.2 ± 4.7	
SM	236[b]			
PC/SM/PA (66 : 30 : 4)	(234)	(39)	(71.5)	255
SM/CL/PA (48 : 48 : 4)	(362)	(45)	(113.2)	530

Δr ≡ membrane thickness (Johnson, 1973); *V*/*A* ≡ volume/area ratio (*see* Materials and Methods). PC ≡ phosphatidylcholine; PA ≡ phosphatidic acid; CL ≡ cholesterol; SM ≡ sphingomyelin. Parentheses indicate dimensions estimated assuming SM has identical properties to those of PC.
[a] Johnson (1973).
[b] Schmidt, Barenholz and Thompson (1977).

Solute Uptake Follows Exponential Kinetics

Uptake curves such as Fig. 1*a* for MTA in PC/CL/PA liposomes were fitted to a single exponential as described in Todd et al. (1989). The data was transformed by subtracting each data point from a data point at a fixed later time (δt = 20 sec in this case), yielding an exponential decay that was fitted to two parameters by nonlinear least squares. A semilog plot of the decay curve is shown in Fig. 1*b*. Note that later times are quite noisy, but that earlier times give a convincingly linear plot. For faster time constants, the semilog plot is potentially useful in defining the period of mixing. Early points, which deviate from a straight line, correspond to the period of mixing.

Only Neutral Amine Permeates

In our analysis (Todd et al., 1989), we assume that the charged form of the amine is impermeant on the time scale of our experiments. We justify this assumption by the fact that CAT_1, a permanently charged cation, does not enter liposomes to a detectable extent over a period of several hours.

The Unstirred Layer Is Not Rate Limiting

In the preceding paper, we extracted the unstirred layer permeability for red cells in our stopped-flow apparatus from the pH dependence of the measured permeability of DMTA. We did not repeat this procedure with sonicated liposomes because equilibration of MTA (our fastest resolvable probe in PC/PA

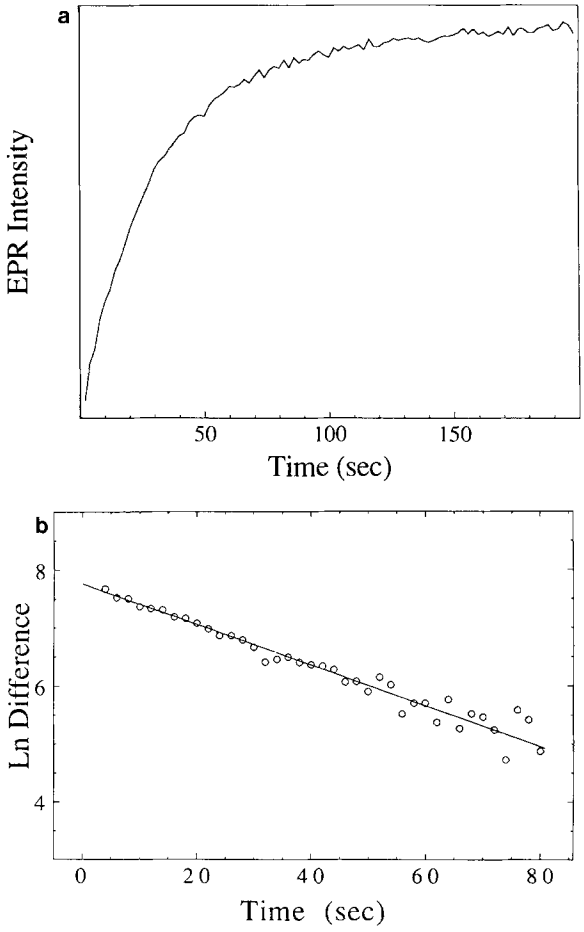

Fig. 1. (*a*) Time course of low field peak upon rapid mixing of MTA in quenching buffer (pH 4) with PC/CL/PA liposomes suspended in citrate buffer (pH 4). (*b*) Semilog plot of $\delta E(t, \delta t)$ for MTA influx into PC/CL/PA liposomes (Fig. 1*a*). δt = 20 sec. Slope = −0.0317 ± 0.0011 sec^{-1}. This implies a time constant τ = 31.5 sec

Table 2. Amine spin probe permeabilities in sonicated liposomes (pH 4.0)

	$P \times 10^3$	P/P_{calc}
PC/PA (96:4)		
META	4.14 ± 1.21	0.11
TA	2.94 ± 0.65	0.047
MTA	9.21 ± 2.04	0.046
PC/CL/PA (70:26:4)		
META	0.641 ± 0.106	0.017
TA	0.838 ± 0.142	0.013
MTA	2.03 ± 0.33	0.010
DMTA	8.87 ± 1.70	0.0069
PC/SM/PA (66:30:4)		
TA	1.89 ± 0.46	0.03
MTA	6.90 ± 1.66	0.034
SM/CL/PA (48:48:4)		
DMTA	0.0557 ± 0.0066	0.000043

$P_{calc} \equiv KD/\Delta r$; $K = K_{hex}$; $D = 10^{-6}$ cm²/sec; $\Delta r = 5 \times 10^{-7}$ cm.

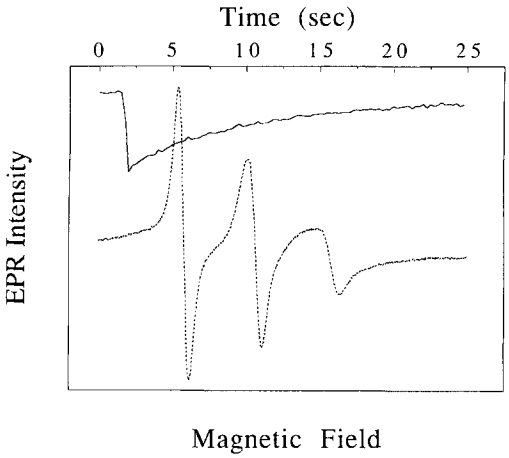

Fig. 2. Kinetics of membrane-bound TA distribution across PC/PA liposomes suspended in a buffer combining quenching buffer 1:1 with citrate buffer (pH 4). [TA] = 1 mM. Dashed line: equilibrium spectrum for TA in liposomes suspended in same buffer, scan width = 83 gauss. Solid line: time course of low field peak upon rapid mixing of liposomes with TA

liposomes) becomes too fast for good resolution above pH 4 and phospholipid vesicles become unstable at more acid pH values. Instead, we estimate a lowerbound for the unstirred layer permeability in this system by assuming that the entire extravesicular volume is unstirred, with liposomes distributed evenly throughout the volume of the suspension (i.e., perfect mixing). Let each liposome be centered in an equal spherical volume of radius d_{ul}. For a 25 mg/ml suspension of PC/PA (96:4) liposomes, assuming a weight of 4.8×10^{-18} g/liposome (Johnson, 1973), we calculate an extravesicular volume/liposome of 1.9×10^{-16} cm³. This corresponds to $d_{ul} = 3.6 \times 10^{-6}$ cm. For a diffusion coefficient of 10^{-5} cm²/sec, we calculate $P_{ul} = D/d_{ul} = 2.8$ cm/sec. This is about two orders of magnitude faster than the permeabilities we have measured for three amines in PC/PA liposomes (Table 2). Since measured permeabilities are even lower for liposomes of other compositions, we conclude that unstirred layers *per se* cannot have affected our results.

Incomplete mixing could conceivably create an effective unstirred layer thickness that is much greater than the theoretical one we have calculated above. If, in the worst possible case, there were no mixing (the two solutions each occupy opposite halves of the glass capillary within the cavity), we would have an average unstirred layer thickness of about 0.05 cm (the radius of the capillary), which corresponds to $P_{ul} = 2 \times 10^{-4}$ cm/sec (and a resistance of $1/P_{ul} = 5 \times 10^3$ sec/cm). Since we are operating at some 5 pH units below the amine pK_a, the membrane resistance corresponding to MTA in PC/PA liposomes is approximately 10^7 sec/cm (Eq. (5), Todd et al., 1989), which is still a factor of 2000 greater than the worst case unstirred layer resistance.

Adsorption/Desorption Is Not Rate Limiting

The basic steps in membrane permeation of amine solutes may be broken down as follows. (*i*) Both the charged and the neutral species adsorb to the membrane surface. Given the high pK_a for the amine spin probes (≃9), only one molecule in 10^5 is neutral in the bulk aqueous phase at pH 4. (*ii*) The charged species is converted to the neutral species while bound at the surface by loss of a proton. Protonation/deprotonation is normally assumed to be very fast. (*iii*) The neutral species diffuses across the membrane. (*iv*) The amine desorbs or is protonated and then desorbs at the opposite interface.

When amine spin probe in quencher solution is mixed with liposomes formed in quencher solution, the external and internal aqueous spectra are suppressed and the membrane-bound spectrum is observed (Fig. 2). The kinetics of emergence of the bound spectrum reveal whether the adsorption/desorption rate is fast or slow relative to diffusion across the membrane. As can be seen in Fig. 2, upon rapid mixing of TA in quencher solution with liposomes in quencher solution, approximately half of the equilibrium-bound spectral amplitude arises immediately, while the other half arises slowly and asymptotically. Apparently, probe binds rapidly to the outer leaflet, but much more slowly to the inner leaflet ($\tau \simeq 9$ sec) as the neutral probe diffuses across the membrane. In a similar experiment with

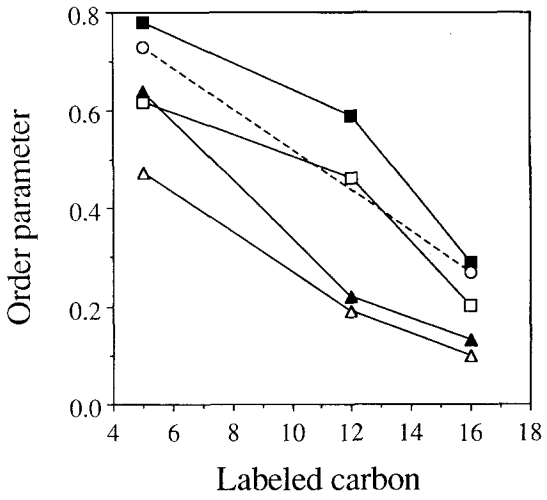

Fig. 3. Apparent order parameters for 5-, 12-, and 16-doxyl stearic acid spin labels in PC/PA (96 : 4) liposomes (open triangles); PC/CL/PA (70 : 26 : 4) liposomes (open squares); PC/SM/PA (66 : 30 : 4) liposomes (filled triangles); SM/CL/PA (48 : 48 : 4) liposomes (filled squares); red cell ghosts (open circles). Ghosts were prepared according to Cabantchik (1981). Stearic acid spin labels were obtained from Syva and Sigma

the fast permeating nitroxide spin probe, TEMPO, only a short transient was observed, with an equilibration time of ≃150 msec (*data not shown*), which places an upper limit on the combined mixing and unstirred layer equilibration times. Therefore, the rate-limiting step for TA cannot be adsorption/desorption at the interface or diffusion across the unstirred layer, but at some step in its diffusion across the membrane. We obtained similar results for MTA in PC/PA liposomes and for TA in PC/CL/PA liposomes at pH 4. In all other cases, binding of probe to the membrane was insufficient to make such a determination.

Permeability Varies with Lipid Composition

The measured permeabilities for the four amine probes at pH 4 in liposomes of different composition are given in Table 2. It can be seen that the permeabilities are fastest for PC/PA liposomes, somewhat slower for PC/CL/PA and PC/SM/PA liposomes, and are by far the slowest for SM/CL/PA liposomes. It was necessary to operate at this low pH in order to slow the probe kinetics to accommodate the time resolution limitations of our stopped-flow mixing apparatus and A/D converter. These same limitations precluded measurement of carboxylate spin probe permeabilities (Todd et al., 1989) because of the high pH (>9) necessary for time resolution of these probes. At such a high pH, lipid is seriously degraded by both oxidation and hydrolysis during sonication.

Membrane Order Depends On Lipid Composition

The apparent order parameter, S_{app}, for 5-, 12-, and 16-doxyl stearic acids in liposomes of various composition was calculated according to Griffith and Jost (1976) (Fig. 3). The order parameters for red cell ghosts are included for comparison. The value for the 12-doxyl label could not be obtained in ghost membranes because of its poor partitioning into these membranes. It can be seen that in all membranes there is a decrease in order toward the terminal methyl groups of the acyl chains. The pattern for PC/SM/PA liposomes is somewhat anomalous, however, because they are highly ordered at the fifth carbon position (similar to PC/CL/PA liposomes) but very disordered at the 12 and 16 carbons (similar to PC/PA liposomes).

TEMPO Membrane Solubility Depends On Lipid Composition

In evaluating the solubility-diffusion mechanism of permeation, it is useful to have some measure of solute solubility in the hydrocarbon region of the membrane. For the polar nonelectrolytes employed in this study, this is problematic since amphiphiles are believed to partition predominantly to the region of the polar head groups (Diamond & Katz, 1974) and reveal very little about solubility in the hydrocarbon region.

To observe the effect of lipid composition on solubility in the hydrocarbon region of the membrane, we measured the membrane partitioning of a hydrophobic analog of the amine spin probes. "TEMPO" is the nitroxide moiety of structure I ($R = H$) in the previous paper. It is believed to partition mainly to the fluid hydrocrbon region of the membrane because of its high bulk hydrocarbon solubility ($K_{hex} = 29.6$ at 25°C) and because its membrane spectrum reflects isotropic motion (Hubbell & McConnell, 1968).

Membrane/water partition coefficients may be extracted from composite spectra of TEMPO in aqueous membrane suspensions. Such a composite spectrum (high field peak only) is shown in Fig. 4 for PC/PA liposomes. Since the membrane and aqueous peaks are partially distinguishable, the spectrum for each phase may be obtained by spectral subtraction. The amount of spin in each phase is then obtainable by double integration. For convenience, we measured instead a TEMPO "solubility

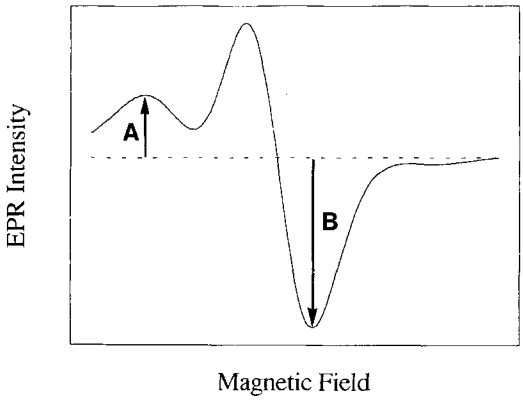

Fig. 4. TEMPO membrane/aqueous spectrum (high field peak) in sonicated PC/PA (96 : 4) liposomes, pH 4.0. [Lipid] = 26.5 mg/ml; [TEMPO] = 0.2 mM. Dashed line is baseline (zero signal). Scan range = 8 gauss

parameter" (Shimshick & McConnell, 1973), which correlates with the membrane/water partition coefficient. For the spectrum in Fig. 4, the amplitude "A" is proportional to the concentration of probe in the membrane phase while the amplitude "B" is proportional to the concentration of probe in the aqueous phase. We define the solubility parameter as $A/(A + B) - A_0/(A_0 + B_0)$ where A_0 and B_0 are the amplitudes for a purely aqueous spectrum.

We have measured this parameter for liposome membranes of varied composition and for red cell ghosts (Table 3). By comparing these results with Fig. 3, it can be seen that TEMPO solubility in the fluid hydrocarbon region of the membrane roughly parallels membrane disorder.

Permeability and Solubility in Nonpolar Solvents

In the second column of Table 2, our measured permeabilities are compared with the estimated permeability for a sheet of hexadecane 50 A thick. It can be seen that in all cases the measured permeability is much lower ($P/P_{calc} \ll 1$). This is in contrast to the results of Finkelstein (1976) and data compiled by Walter and Gutknecht (1986) (Table 4) for egg PC-decane planar lipid bilayers. It has been suggested that egg PC-decane planar bilayers may contain significant amounts of decane (Orbach & Finkelstein, 1980). If so, this might explain why hexadecane is a better model solvent for these membranes than for solvent-free egg PC liposomes. There is accumulating evidence that the solubility of nonelectrolytes is greater in bulk hydrocarbon than in lipid bilayers.

Table 3. TEMPO partitioning parameter (pH 4.0)

	Per mg lipid	Per mg phospholipid
PC/PA (96 : 4)	0.0088	0.0088
PC/CL/PA (66 : 30 : 4)	0.0035	0.0048
SM/CL/PA (48 : 48 : 4)	0.0020	0.0038
RBC ghosts[a]	0.0020	0.0026

T = 17–25°C.
[a] Percentage of total ghost weight that is lipid and phospholipid was taken from Pennell (1974).

Table 4. Solute permeabilities in egg PC-decane planar lipid bilayers (P, K_{hex} compiled by Walter & Gutknecht, 1986)

	$P \times 10^2$	P/P_{calc}
1. Water	0.34	4.0
2. Hydrofluoric acid	0.031	3.7
3. Ammonia	13.0	3.0
4. Hydrochloric acid	290.0	2.4
5. Formic acid	0.73	3.3
6. Methylamine	8.0	0.73
7. Formamide	0.01	0.63
8. Nitric acid	0.092	0.67
9. Urea	0.0004	0.71
10. Thiocyanic acid	260.0	0.41
11. Acetic acid	0.69	0.65
12. Ethylamine	12.0	0.46
13. Ethanediol	0.0088	0.26
14. Acetamide	0.017	0.40
15. Propionic acid	3.5	0.76
16. 1,2-Propanediol	0.028	0.22
17. Glycerol	0.00054	0.14
18. Butyric acid	9.5	0.55
19. 1,4-Butanediol	0.027	0.31
20. Benzoic acid	55.0	0.52
21. Hexanoic acid	110.0	0.39
22. Salicylic acid	77.0	0.64
23. Codeine	14.0	0.17

$P_{calc} = KD/\Delta x$; $K = K_{hex}$; $D = 10^5$ cm^2/sec; $\Delta x = 50$ A.

For example, Simon, Stone and Busto-Latorre (1977) found that the enthalpy and entropy of partition for one solute (hexane) between bulk hydrocarbon and egg PC liposomes both differ significantly from zero, from which they concluded that bulk hydrocarbon is a poor model for lipid bilayers.

Permeability in PC/CL/PA liposomes is plotted against hexadecane/water and octanol/water partition coefficients (K_{hex} and K_{oct}, respectively) in Fig. 5*a* and *b*. It can be seen that while both plots yield convincing straight lines, they depart significantly

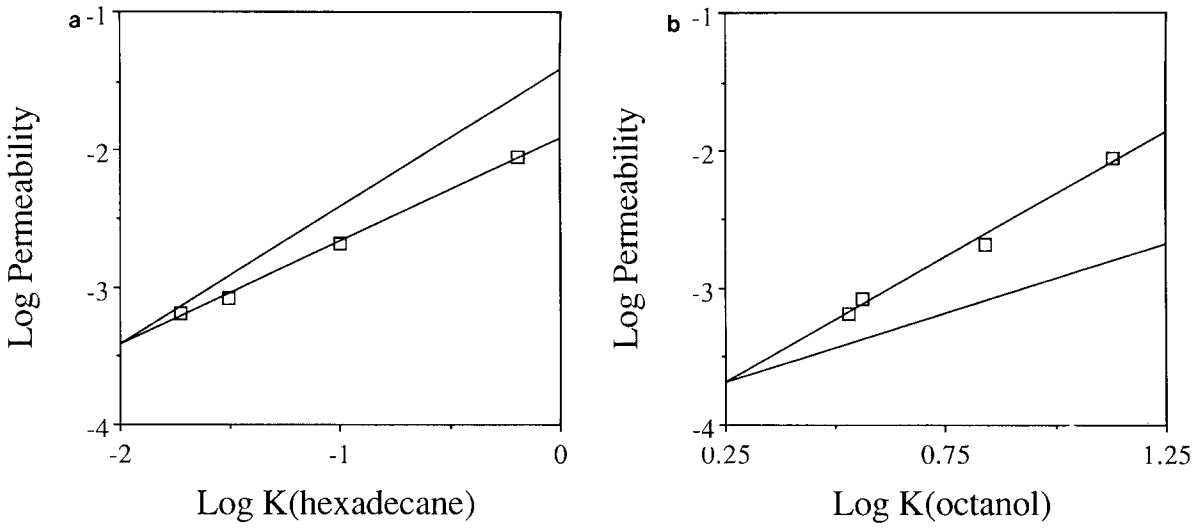

Fig. 5. (*a*) Permeability of PC/CL/PA liposomes, pH 4.0 *vs.* hexadecane/water partition coefficient. Lower line is least squares regression line with slope = 0.75 ± 0.03. Upper line has unity slope. (*b*) Permeability of PC/CL/PA liposomes, pH 4.0 *vs.* octanol/water partition coefficient. Upper line is least squares regression with slope = 1.83 ± 0.14. Lower line has unity slope

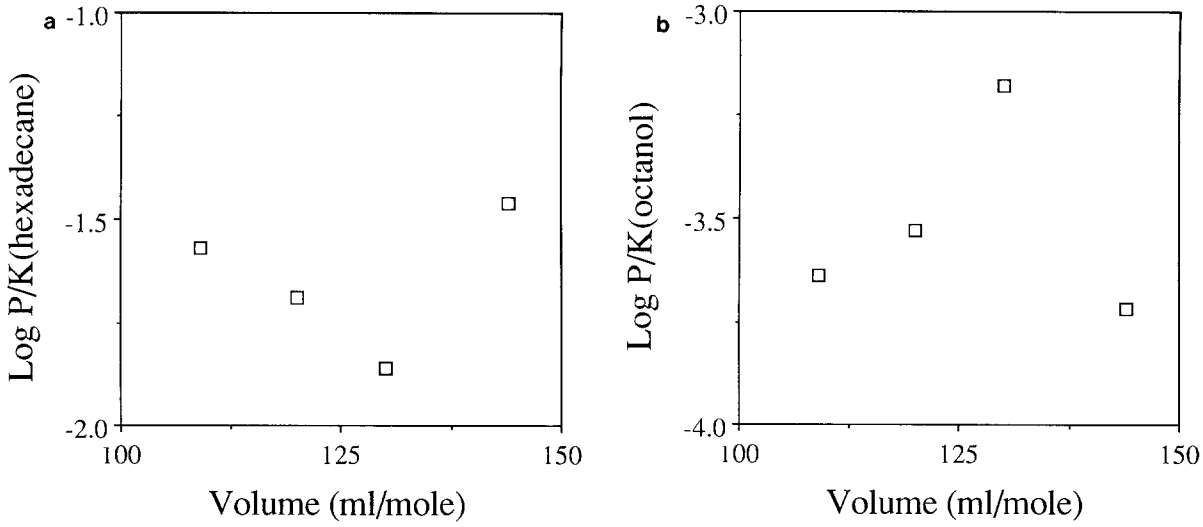

Fig. 6. (*a*) Volume dependence of permeability in PC/CL/PA liposomes, corrected for *n*-hexadecane/water partitioning. (*b*) Volume dependence of permeability in PC/CL/PA liposomes, corrected for 1-octanol/water partitioning

from the slope of unity expected for the "correct" model solvent assuming a solubility-diffusion mechanism of permeation. The plot *vs.* K_{hex} has a slope of 0.75 ± 0.03, while the plot *vs.* K_{oct} has a slope of 1.83 ± 0.14. These slopes are strikingly similar to those found for the same probes in human red cells: 0.73 ± 0.02 and 1.76 ± 0.16, respectively (Todd et al., 1989), though the magnitudes of the permeabilities are greater in this case.

No Apparent Size Dependence of Permeability

Permeability is not a simple function of molecular volume for the amine probes in PC/Cl/PA membranes, as can be seen in Fig. 6*a* and *b*. The "hydrophobicity" contribution to the permeability has been removed by dividing by K_{hex} or K_{oct}, following Wolosin and Ginsburg (1975). This small data set

does not lend support to a simple free-volume theory of permeation, as was found for the same solutes in human red cells (Todd et al., 1989), but again, only a narrow range of molecular volumes is represented.

Discussion

Interfacial *vs.* Intramembrane Rate Limitation

We have demonstrated that the rate-limiting step in permeation for TA and MTA in PC/PA liposomes as well as TA in PC/CL/PA liposomes, all at pH 4, is diffusion within the membrane and not adsorption/desorption at the aqueous/membrane interface. To our knowledge, this has not previously been proven for a nonelectrolyte. Previously observed correlations of membrane permeability with solubility in hydrophobic solvents are also entirely consistent with an activation energy barrier for adsorption/desorption at the interface (Diamond & Wright, 1969). However, the finding that glycerol and erythritol permeate faster in liposomes composed of phosphatidylcholines with shorter side chains or containing double bonds also strongly suggests a rate-limiting barrier within the membrane (deGier et al., 1968). Once the relevance of the solubility-diffusion model is established, it is then appropriate to interpret our permeability data in terms of the properties of the membrane interior. However, the location of the rate-limiting barrier may well be different for other solutes and/or other membranes.

At pH 4, the amine spin probes are mostly in their ionic form, yet bind to PC/PA (Fig. 3) and PC/CL/PA liposomes. Therefore, they most likely adsorb to the interface as ions under the conditions of our experiment. The adsorption rates for two other spin-labeled ions to membranes have previously been shown to be relatively fast, consistent with our results. Cafiso and Hubbell (1982) found that a spin-labeled phosphonium ion adsorbed to sonicated egg PC liposomes within the mixing time of their stopped-flow apparatus (<40 msec) and that the rate of permeation was limited by intramembrane diffusion of the molecule. Carmeli, Quintanilha and Packer (1980) measured the on-time of CAT_{12} (a longer alkyl chain homolog of CAT_1) to be <7 msec in the purple membrane of halobacteria.

Spin probes have also been exploited in the investigation of interfacial rates for nonelectrolytes in liposome suspensions at equilibrium. A minimum transit time, τ_i, between fluid membrane and aqueous phases was calculated for three nitroxide spin probes, DTBN, TEMPO, and TEMPone in DPPC liposomes from the observed separation of the high field aqueous and membrane-bound spectral peaks (Dix, Diamond & Kivelson, 1974), (Dix, Kivelson & Diamond, 1978). $\tau_i \simeq 10^{-7}$ sec for all three probes. While Dix et al. do not measure permeabilities for the three probes, we can, for example, compare this to the time constant for MTA permeation in PC/PA (pH 4) liposomes: $\tau = V/PA \simeq 5 \times 10^{-5}$ sec, which is comfortably within this constraint.

Dix et al. showed that this minimum transit time cannot be accounted for by the time it takes for a probe molecule to diffuse from the center of the bilayer to the water phase, assuming a homogeneous membrane. This time should be given approximately by: $\tau_D = \Delta x^2/8D \simeq 10$ nsec, where "D" is the diffusion coefficient in the fluid bilayer center for the three probes as measured by EPR (Dix et al., 1974, 1978). Since $\tau_D \ll \tau_i$, they concluded that the minimum transit time must be due either to diffusion through a region of low D in the membrane periphery or to crossing the aqueous/membrane interface.

Dix et al. (1978) converted τ_i to an interfacial resistance with the arbitrary assumption that this resistance corresponds to the polar region of the membrane with thickness $y = 5$ Å. A lowerbound for the interfacial resistance is then $\tau_i/y = 2$ sec/cm. This resistance was then compared to resistances estimated assuming a homogeneous solubility-diffusion barrier. K and D were values for DPPC liposomes at 50°C (above the DPPC phase transition) and presumably reflect values for the center of the bilayer. A hydrocarbon thickness of 30 Å was assumed. A fourth probe, Benzoloxy TEMPO, was included in this comparison under the assumption that it was constrained by the same minimum interphase transit time. It was found that in all four cases the estimated solubility-diffusion resistance was one or more orders of magnitude less than the minimum interfacial resistance from which they concluded that the interface is rate limiting for all four of these probes. We believe this conclusion is correct if it is recognized that their calculated solubility-diffusion resistance reflects only the contribution of the fluid bilayer center and that their "interfacial" resistance must include not only adsorption/desorption at the interface but also diffusion through peripheral regions of the membrane.

The Location of the Intramembrane Resistance

In discussing the permeability of a heterogeneous membrane we find the continuum formalism of Dia-

mond, Szabo and Katz (1974) to be particularly useful as it allows us to conceptually tease apart the components of resistance to permeation and how they are expected to vary across the bilayer. Neglecting the resistances to adsorption and desorption at the aqueous/membrane interface:

$$\frac{1}{P} = \int_0^{\Delta x} \frac{dx}{K(x)D(x)}$$

where $P \equiv$ permeability, $x \equiv$ coordinate normal to the plane of the membrane, $\Delta x \equiv$ membrane thickness, $K(x) \equiv$ position-dependent membrane/water partition coefficient, and $D(x) \equiv$ position-dependent diffusion coefficient. Obviously, the resistance will be at a maximum at the position where the product $K(x)D(x)$ is at a minimum. Unfortunately, we are unable to measure $K(x)$ and $D(x)$. ($D(x)$ could be accurately measured by ^{13}C NMR only if $K(x)$ were known.) Further, the minima for $K(x)$ and $D(x)$ quite possibly do not coincide.

For conceptual purposes we may break down $K(x)$ into two components: dielectric and steric effects. Dielectric effects correspond to the partitioning selectivity of the membrane on the basis of solute polarity. *Steric effects* include changes in entropy of the solute between water and the membrane as well as perturbations of the membrane caused by the partitioning of solute. Steric effects are manifested by the decreasing partition of solutes into membranes of increasing order.

The dielectric component of $K(x)$ obviously depends on the dielectric profile across the membrane and this is not known in detail. However, the current consensus is that $\varepsilon \simeq 2$ from the center of the bilayer out to about the level of the carbonyl groups (Flewelling & Hubbell, 1986). Between the carbonyl groups and the surrounding water, ε rises to ~80. Clearly then, hydrophobicity has a broad maximum and the dielectric component of $K(x)$ has a broad minimum in the center of the bilayer.

$D(x)$ and the steric component of $K(x)$ will be functions of lipid dynamics. Both the amplitude and frequency of lipid acyl chain motions increase from the glycerol backbone to the terminal methyl groups. A gradient in order parameter, which reflects the amplitude of acyl chain motions, has been determined by spin label EPR (Hubbell & McConnell, 1971), deuterium NMR (Seelig & Seelig, 1974), and ^{13}C NMR methods (Lee et al., 1976). A gradient in T_1 for ^{13}C lipid nuclei, reflecting the frequency of nuclear motions, has also been measured for DPPC liposomes (Levine et al., 1972; Godici & Landsberger, 1974). It is reasonable to expect that both $D(x)$ and the steric component of $K(x)$ will increase in a parallel fashion. Regions of the membrane with the greatest amplitude and frequency of lipid acyl chain motions should most easily accommodate a partitioning or diffusing solute. We have shown that the hydrophobic spin probe, TEMPO, has decreased solubility in membranes of increasing order. Dix et al. (1978) measured $D(x)$ for DTBN in DPPC membranes by the ^{13}C-NMR relaxation enhancement of the lipid nuclei. As expected, $D(x)$ increased toward the center of the bilayer, though the steepness of the gradient in $D(x)$ was probably underestimated because of their assumption that probe was distributed evenly throughout the entire bilayer volume.

Given our qualitative understanding of how the functions $K(x)$ and $D(x)$ are likely to vary across the bilayer, we can make a reasonable prediction as to where the product $K(x)D(x)$ reaches a minimum and thereby predict the approximate location of the rate-limiting step. While the dielectric component of $K(x)$ reaches a broad minimum in the center of the bilayer, it should remain low out as far as the carbonyl groups and possibly out to the glycerol backbone (Flewelling & Hubbell, 1986). It is in this region that the steric component of $K(x)$ and $D(x)$ will have a deep minimum (relative to the center of the bilayer). It is therefore likely that the product $K(x)D(x)$ reaches a minimum somewhere in the relatively ordered acyl chain segments near the glycerol backbone.

Our experimental results suggest that this is indeed where the minimum for $K(x)D(x)$ occurs. We have seen that measured spin probe permeabilities in liposomes and red cells (Todd et al., 1989) are an order of magnitude or more slower than permeabilities calculated for a 50-*A* thick sheet of hexadecane. Thus, the maximum resistance is unlikely to be in a region of fluid lipid resembling bulk hydrocarbon. Plots of amine permeability in PC/CL/PA liposomes *vs.* K_{hex} and amine permeability in red cells *vs.* K_{hex} both yield a slope significantly less than one, also contrary to the predictions of the hexadecane sheet model. Similar plots with K_{oct} also deviate from a slope of one, but with a greater slope. This implies that the slope would be one for some solvent intermediate in polarity between hexadecane and octanol. Thus, we may infer that the region of the rate-limiting step in permeation corresponds to a dielectric constant intermediate between hexadecane (ε = 2.1) and octanol (ε = 10.3). This most likely corresponds to the acyl chain segments near the glycerol backbone.

Further support for this assignment is found in the relationship between permeability and the position-dependence of membrane order. It has previously been suggested that since cholesterol has the smallest effect on membrane order for stearic acids spin-labeled at the 16-carbon position, this is un-

likely to be the locus of the increased resistance to permeation observed for cholesterol-containing liposomes (Cohen, 1975*b*). This is also true for order parameters determined by NMR (Taylor & Smith, 1980). We see in Fig. 3 that for all membranes in the present study, the increase in order from that of PC/PA liposomes is least at the 16-carbon position. Sphingomyelin/phosphatidylcholine (PC/SM/PA) liposomes are particularly striking in this regard. As was pointed out previously, these liposomes are highly ordered at the 5-carbon position, which is similar to PC/CL/PA liposomes, while relatively disordered at the 12- and 16-carbon positions, with values similar to PC/PA liposomes. Since these liposomes are more impermeable to our nitroxide probes than PC/PA liposomes, we infer that the rate-limiting barrier is likely to be nearest the 5-carbon position.

Finally, Dix et al. (1978) have shown that the "interfacial" resistance to permeation (including the resistances for adsorption and desorption at the interface as well as the resistance for diffusion through the membrane periphery) for four nitroxide spin probes in DPPC liposomes is likely to be greater than the resistance encountered in the fluid center of the bilayer. We have shown, on the other hand, that the two amine nitroxides, TA and MTA, are not rate limited by adsorption/desorption at the interface in PC/PA liposomes. Together these results strongly suggest that the principal resistance in permeation for these nitroxide probes lies in the membrane periphery, i.e., in the acyl chain segments near the glycerol backbone.

This work was supported by NIH Grant Nos. GM-18819, HL-37593 (to RIM) and AG-04818 (to RJM).

References

Cabantchik, Z.I. 1981. Isolation and reconstitution of band 3, the anion transporter of the human red blood cell membrane. *In:* Membrane Proteins: A Laboratory Manual. A. Azzi, U. Brodbeck, and P. Zahler, editors. pp. 135–152. Springer-Verlag, Berlin

Cafiso, D.S., Hubbell, W.L. 1982. Transmembrane electrical currents of spin-labeled hydrophobic ions. *Biophys. J.* **39**:263–272

Carmeli, C., Quintanilha, A.T., Packer, L. 1980. Surface charge changes in purple membranes and the photoreaction cycle of bacteriorhodopsin. *Proc. Natl. Acad. Sci. USA* **77**:4707–4711

Castle, J.D., Hubbell, W.L. 1976. Estimation of membrane surface potential and charge density from the phase equilibrium of a paramagnetic amphiphile. *Biochemistry* **15**:4818–4831

Cohen, B.E. 1975*a*. The permeability of liposomes to nonelectrolytes I: Activation energies for permeation. *J. Membrane Biol.* **20**:205–234

Cohen, B.E. 1975*b*. The permeability of liposomes to nonelectrolytes. II: The effect of nystatin and gramicidin A. *J. Membrane Biol.* **20**:235–268

Cohen, B.E., Bangham, A.D. 1972. Diffusion of small non-electrolytes across liposome membranes. *Nature (London)* **236**:173–174

Diamond, J.M., Katz, Y. 1974. Interpretation of nonelectrolyte partition coefficients between dimyristoyllecithin and water. *J. Membrane Biol.* **17**:121–154

Diamond, J.M., Szabo, G., Katz, Y. 1974. Theory of nonelectrolyte permeation in a generalized membrane. *J. Membrane Biol.* **17**:148–152

Diamond, J.M., Wright, E.M. 1969. Biological membranes: The physical basis of ion and nonelectrolyte selectivity. *Annu. Rev. Physiol.* **31**:581–646

Dix, J.A., Diamond, J.M., Kivelson, D. 1974. Translational diffusion coefficient and partition coefficient of a spin-labeled solute in lecithin bilayer membranes. *Proc. Natl. Acad. Sci. USA* **71**:474–478

Dix, J.A., Kivelson, D., Diamond, J.M. 1978. Molecular motion of small nonelectrolyte molecules in lecithin bilayers. *J. Membrane Biol.* **40**:315–342

Duggleby, R.G. 1981. A nonlinear regression program for small computers. *Anal. Biochem.* **110**:9–18

Finkelstein, A. 1976. Water and nonelectrolyte permeability of lipid bilayer membranes. *J. Gen. Physiol.* **68**:127–135

Finkelstein, A., Cass, A. 1968. Permeability and electrical properties of thin lipid membranes. *J. Gen. Physiol.* **52**:145s–172s

Flewelling, R.F., Hubbell, W. L. 1986. The membrane dipole potential in a total membrane potential model. *Biophys. J.* **49**:541–552

Gier, J. de, Mandersloot, J.G., Deenen, L.L.M. van. 1968. Lipid composition and permeability of liposomes. *Biochim. Biophys. Acta* **150**:137–155

Godici, P.E., Landsberger, F.R. 1974. The dynamic structure of lipid membranes. A ^{13}C nuclear magnetic resonance study using spin labels. *Biochemistry* **13**:362–368

Griffith, O.H., Jost, P.C. 1976. Lipid spin labels in biological membranes. *In:* Spin Labeling, Theory and Applications. L.J. Berliner, editor. pp. 453–523. Academic, New York

Huang, C., Mason, J.T. 1978. Geometric packing constraints in egg phosphatidylcholine vesicles. *Proc. Natl. Acad. Sci. USA* **75**:308–310

Hubbell, W.L., McConnell, H.M. 1968. Spin-label studies of the excitable membranes of nerve and muscle. *Proc. Natl. Acad. Sci. USA* **61**:12–16

Hubbell, W.L., McConnell, H.M. 1971. Molecular motion in spin-labeled phospholipids and membranes. *J. Am. Chem. Soc.* **93**:314–326

Johnson, S.M. 1973. The effect of charge and cholesterol on the size and thickness of sonicated phospholipid vesicles. *Biochim. Biophys. Acta* **307**:27–41

Kates, M. 1972. Techniques of lipidology; isolation, analysis, and identification of lipids. North-Holland, Amsterdam

Lanczos, C. 1956. Applied Analysis. Prentice-Hall, Englewood Cliffs (NJ)

Lee, A.G., Birdsall, N.J.M., Metcalfe, J.C., Warren, G.B., Roberts, G.C.K. 1976. A determination of the mobility gradient in lipid bilayers by ^{13}C nuclear magnetic resonance. *Proc. R. Soc. London B* **193**:253–274

Levine, Y.K., Birdsall, N.J.M., Lee, A.G., Metcalfe, J.C. 1972. ^{13}C nuclear magnetic resonance relaxation measurements of synthetic lecithins and the effect of spin-labeled lipids. *Biochemistry* **11**:1416–1421

Lieb, W.R., Stein, W.D. 1969. Biological membranes behave as

non-porous polymeric sheets with respect to the diffusion of non-electrolytes. *Nature (London)* **224:**240–243

Lieb, W.R., Stein, W.D. 1971. The molecular basis of simple diffusion within biological membranes. *In:* Current Topics in Membranes and Transport. F. Bronner and A. Kleinzeller, editors. pp. 1–39. Academic, New York

Lieb, W.R., Stein, W.D. 1986. Non-stokesian nature of transverse diffusion within human red cell membranes. *J. Membrane Biol.* **92:**111–119

Orbach, E., Finkelstein, A. 1980. The nonelectrolyte permeability of planar lipid bilayer membranes. *J. Gen. Physiol.* **75:**427–436

Pennell, R.B. 1974. Composition of normal human red cells. *In:* The Red Blood Cell. D.M. Surgenor, editor. pp. 93–97. Academic, New York

Schmidt, C.F., Barenholz, Y., Thompson, T.E. 1977. A nuclear magnetic resonance study of sphingomyelin in bilayer systems. *Biochemistry* **16:**2649–2656

Seelig, A., Seelig, J. 1974. The dynamic structure of fatty acyl chains in a phospholipid bilayer measured by deuterium magnetic resonance. *Biochemistry* **13:**4839–4845

Shimshick, E.J., McConnell, H.M. 1973. Lateral phase separations in binary mixtures of cholesterol and phospholipids. *Biochem. Biophys. Res. Commun.* **53:**446–451

Simon, S.A., Stone, W.L., Busto-Latorre, P. 1977. A thermodynamic study of the partition of *n*-hexane into phosphatidylcholine and phosphatidylcholine-cholesterol bilayers. *Biochim. Biophys. Acta* **468:**378–388

Singleton, W.S., Gray, M.S., Brown, M.L., White, J.L. 1965. Chromatographically homogeneous lecithin from egg phospholipids. *J. Am. Oil. Chem. Soc.* **42:**53–56

Taylor, M.G., Smith, I.C.P. 1980. The fidelity of response by nitroxide spin probes to changes in membrane organization: The condensing effect of cholesterol. *Biochim. Biophys. Acta* **599:**140–149

Todd, A.P., Mehlhorn, R.J., Macey, R.I. 1989. Amine and carboxylate spin probe permeability in red cells. *J. Membrane Biol.* **109:**41–52

Walter, A., Gutknecht, J. 1986. Permeability of small nonelectrolytes through lipid bilayer membranes. *J. Membrane Biol.* **90:**207–217

Wolosin, J.M., Ginsburg, H. 1975. The permeation of organic acids through lecithin bilayers: Resemblance to diffusion in polymers. *Biochim. Biophys. Acta* **389:**20–33

Received 19 September 1988; revised 3 January 1989

Appendix

Flux Kinetics for Suspensions of Heterogeneously-Sized Vesicles

A common experimental problem in membrane transport is measuring solute permeabilities for a suspension of heterogeneously-sized vesicles. To a first approximation, permeability will not depend on the size of the vesicles, but the time course of equilibration will. For instance, we may attempt to determine the vesicle permeability of a solute by curve fitting the time course of uptake after rapid mixing of the solute with a suspension of vesicles. If the vesicles are of uniform size, equilibration will proceed monoexponentially, with the time constraint depending on the volume/area ratio, the concentration of vesicles, and inversely with the permeability. For a suspension of N populations of vesicles of discrete sizes, however, equilibration will proceed as the sum of N exponentials. For a narrow size dispersion, we may calculate an approximate permeability by assuming that all vesicles are of average size and fitting to a single exponential. However, for very disperse vesicle distributions, this procedure fails as the time course is biased by the larger, slowly filling vesicles. In this section, we develop the mathematical description of this problem and show how the true permeability may be determined if the vesicle size distribution is known.

Single Population Case

We consider the equilibration of a neutral solute in a suspension of vesicles of uniform size. For this special case, Eq. (1) in the previous paper (Todd et al., 1989) reduces to

$$\frac{ds_{in}}{dt} = \frac{PA}{V(1-f)}\left(f - s_{in}\right) \tag{A1}$$

where $s_{in} \equiv$ number of internal solute molecules/total number of solute molecules, $P \equiv$ solute permeability, $A \equiv$ vesicle surface area, $V \equiv$ vesicle internal volume, and $f \equiv$ internal volume/total aqueous volume.

If we assume that the vesicles are spherical and large enough so that the inner and outer radii are virtually equal, we also have

$$A/V = 3/r \tag{A2}$$

where "r" is the vesicle radius. Making this substitution we get

$$\frac{ds_{in}}{dt} = \frac{3P}{r(1-f)}\left(f - s_{in}\right) \tag{A3}$$

which has the solution

$$s_{in}(t) = f(1 - e^{-t/\tau}).$$
$$\tau = r(1-f)/3P. \tag{A4}$$

It is apparent that equilibration will proceed more slowly for dilute suspensions of large vesicles.

Multiple Populations

For a suspension of N discrete vesicle sizes, the flux expression for each population is:

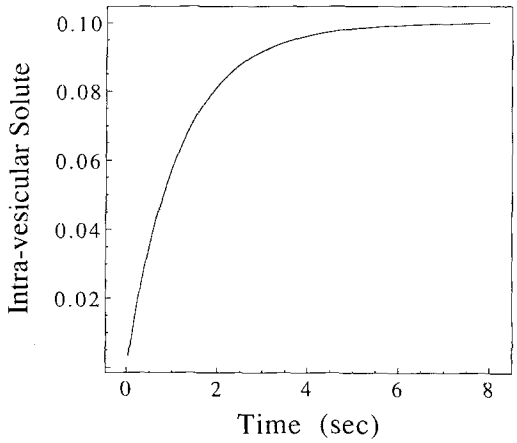

Fig. A1. Aggregate influx for 10 Gaussian-distributed populations. Mean radius = 1 cm. SD = 0.3 cm

Table A1. Error in computed permeability for Gaussian vesicle radius distribution

SD (%)	$r_{eff} = r_{av}$ % error in P	$r_{eff} = r_{Vmax}$ % error in P
5	−0.1	+0.8
10	−1.7	+1.1
15	−4.4	+1.7
20	−7.7	+2.3
25	−11.4	+2.9
30	−15.4	+3.3
35	−19.3	+3.7
40	−23.2	+4.1
45	−26.8	+4.4

Computed for 10 normally distributed populations with 10% internal volume.

$$\frac{ds_{in}^{(j)}}{dt} = \frac{3P}{r_j}\left(\frac{f_j s_{out}}{(1-f)} - s_{in}^{(j)}\right) \tag{A5}$$

where $s_{in}^{(j)} \equiv$ fraction internal solute for jth population
$s_{out} = 1 - \Sigma s_{in}^{(j)}$
$f = \Sigma f_j$
$f_j \equiv$ fraction vesicle volume for jth population
$r_j \equiv$ vesicle radius for jth population.

In the limit of very dilute suspensions, $s_{out} \simeq 1$, $1 - f \simeq 1$, and Eq. (A5) reduces to the single population case. The aggregate solution will then be a simple sum of exponential solutions for independent populations. For more concentrated suspensions, solution of this problem is more difficult because the fluxes are coupled: the flux of solute into one population will alter the driving force and hence the flux into the other populations and vice versa. The N equations (Eq. (A5)) can still, in principle, be solved by the methods of linear algebra, but this becomes impractical for large N.

Alternatively, these equations may be simultaneously numerically integrated by the Runge-Kutta method. The aggregate solution for the N vesicle populations may then be fitted to a single exponential by nonlinear least squares (Duggleby, 1981). In the following computer simulations for heterogeneous suspensions, the time interval between points was constrained to be short enough so that the numerical solution for a homogeneous suspension of vesicles of the smallest radius could be curve fitted to a time constant within 1% of the actual time constant. At the same time, sufficient points were taken so that the numerical solution for a homogeneous suspension of vesicles of the largest radius could be curve fitted to the same accuracy.

We begin by assuming that the N populations follow a Gaussian distribution about a mean radius. The aggregate numerical solution for solute influx into 10 Gaussian-distributed populations is seen in Fig. A1. If we fit the solution to a single exponential and assume that the "effective" radius is the average radius, we compute a permeability that is too low by 15% for a vesicle distribution with a 30% SD and 10% internal volume. This level of accuracy may be sufficient for many purposes. The deviations of the computed permeability from the true permeability for a range of vesicle distribution standard deviations are given in Table A1. We obtain a somewhat better estimate of the permeability if we assume that the effective radius is the volume-weighted average radius, i.e., the radius at the maximum for the volume fraction distribution. In this case, we calculate a permeability that is too high by only 3.3%. That this approximate calculation is generally very good for Gaussian distributions of vesicle radii can also be seen in Table A1. Setting the effective radius equal to the maximum for the area fraction distribution (weighting by r^2 instead of r^3) works equally well but instead slightly underestimates the true permeability.